The Monitor project: rotation of low-mass stars in the open cluster NGC 2547

Jonathan Irwin,[1,2]⋆ Simon Hodgkin,[1] Suzanne Aigrain,[3] Jerome Bouvier,[4] Leslie Hebb[5] and Estelle Moraux[4]

[1]*Institute of Astronomy, University of Cambridge, Madingley Road, Cambridge CB3 0HA*
[2]*Harvard–Smithsonian Center for Astrophysics, 60 Garden Street, Cambridge, MA 02138, USA*
[3]*Astrophysics Group, School of Physics, University of Exeter, Stocker Road, Exeter EX4 4QL*
[4]*Laboratoire d'Astrophysique, Observatoire de Grenoble, BP 53, F-38041 Grenoble Cédex 9, France*
[5]*School of Physics and Astronomy, University of St Andrews, North Haugh, St Andrews KY16 9SS*

ABSTRACT

We report on the results of an *I*-band time-series photometric survey of NGC 2547 using the MPG/ESO 2.2-m telescope with Wide Field Imager, achieving better than 1 per cent photometric precision per data point over $14 \lesssim I \lesssim 18$. Candidate cluster members were selected from a *V* versus *V − I* colour–magnitude diagram over $12.5 < V < 24$ (covering masses from $0.9\,\mathrm{M_\odot}$ down to below the brown dwarf limit), finding 800 candidates, of which we expect ∼330 to be real cluster members, taking into account contamination from the field (which is most severe at the extremes of our mass range). Searching for periodic variations in these gave 176 detections over the mass range $0.1 \lesssim M/\mathrm{M_\odot} \lesssim 0.9$. The rotation period distributions were found to show a clear mass-dependent morphology, qualitatively intermediate between the distributions obtained from similar surveys in NGC 2362 and 2516, as would be expected from the age of this cluster. Models of the rotational evolution were investigated, finding that the evolution from NGC 2362 to 2547 was qualitatively reproduced (given the uncertainty in the age of NGC 2547) by solid body and core-envelope decoupled models from our earlier NGC 2516 study without need for significant modification.

Key words: techniques: photometric – surveys – stars: rotation – open clusters and associations: individual: NGC 2547.

1 INTRODUCTION

NGC 2547 is a relatively well-studied nearby young open cluster; we adopt the parameters of Naylor & Jeffries (2006), who give an age of $38.5^{+3.5}_{-6.5}$ Myr, distance modulus $(M − m)_0 = 7.79^{+0.11}_{-0.05}$ and reddening $A_V = 0.186$. The age derived by these authors puts the cluster at the approximate point where G-dwarfs reach the zero-age main-sequence (ZAMS; see e.g. fig. 1 of Irwin et al. 2007b), and slightly younger than the typically used benchmark of α Persei (∼50 Myr, e.g. Basri & Martín 1999). The small distance modulus makes it possible to probe down to very low masses, with relatively modest-sized telescopes.

The cluster has been surveyed in X-rays using *ROSAT* (Jeffries & Tolley 1998) and *XMM–Newton* (Jeffries et al. 2006). The latter study found that the solar type stars in NGC 2547 exhibited a similar relation between X-ray activity and Rossby number to field stars and older clusters, but with saturated or supersaturated X-ray

activity levels, and median levels of X-ray luminosity and X-ray to bolometric luminosity ratio similar to T-Tauri stars in the ONC, but much higher than in the Pleiades. These measures are consistent with the relative youth of NGC 2547.

Surveys of lithium depletion (Jeffries et al. 2003; Oliveira et al. 2003; Jeffries & Oliveira 2005) have placed constraints on the cluster age, and conversely, on stellar evolution models by comparison with isochrone-fitting results. Jeffries & Oliveira (2005) find ages based on lithium depletion of 34–36 Myr, reasonably consistent with the isochrone-based estimate we assumed earlier.

Jeffries, Totten & James (2000) performed a $v \sin i$ survey of the solar type stars in the cluster, finding a distribution indistinguishable from that in the similar-age clusters IC 2391 and IC 2602, with a similar rotation–activity relationship to older clusters such as the Pleiades. Littlefair et al. (2003) found weak evidence for mass segregation in the cluster, confirmed by Jeffries et al. (2003) using a new photometric survey, where they also derived the cluster mass function down to ∼0.05 M⊙, finding a result very similar to the Pleiades mass function over the range $0.075 < M/\mathrm{M_\odot} < 0.7$.

⋆E-mail: jmi@ast.cam.ac.uk

Finally, NGC 2547 has been observed with *Spitzer* using the IRAC and MIPS instruments by Young et al. (2004) to investigate the cluster disc frequency. Gorlova et al. (2007) subsequently extended the survey coverage, finding only two to four out of ~600 stars of B–mid-M spectral type to show excesses in the IRAC 8 μm band, a fraction of $\lesssim$ 1 per cent. In the MIPS 24 μm band, they found ~40 per cent of the stars of B–F spectral types to show excesses. This striking result is most likely due to the discs clearing from the inside outwards, with the lack of short-wavelength excesses caused by the discs being substantially cleared within the central ~1 au parts by the age of NGC 2547.

1.1 Evolution of stellar angular momentum

For a discussion of the context of this work, the reader is referred to our M34 and NGC 2516 publications in Irwin et al. (2006) and Irwin et al. (2007b). The present survey probes a different open cluster of younger age (~40 Myr for NGC 2547, compared to ~150 Myr for NGC 2516 and 200 Myr for M34). Due to the small distance modulus and young age, the NGC 2547 survey probes a relatively wide range of masses, covering $0.1 \lesssim M/M_{\odot} \lesssim 0.9$, compared to $0.1 \lesssim M/M_{\odot} \lesssim 0.7$ in NGC 2516 and $0.25 \lesssim M/M_{\odot} \lesssim 1.0$ in M34. This will allow a more detailed comparison with models of angular momentum evolution, and in particular to test our results in Irwin et al. (2007b), where we found that the evolution of the fast rotators appeared to be better reproduced by solid body models, and the slow rotators by differentially rotating models. At the age of NGC 2547, stars with masses $M \lesssim 0.4\,M_{\odot}$ should be fully convective, and at $0.4\,M_{\odot}$, just beginning to develop a radiative core (Chabrier & Baraffe 1997).

1.2 The survey

We have undertaken a photometric survey in NGC 2547 using the MPG/ESO 2.2-m telescope with the Wide Field Imager (WFI; Baade et al. 1999). Our goals are twofold: first, to study rotation periods for a sample of low-mass members, covering K and M spectral types, down to ~0.1 M$_{\odot}$, and secondly, to look for eclipsing binary systems containing low-mass stars, to obtain dynamical mass measurements in conjunction with radial velocities from follow-up spectroscopy. Such systems provide the most accurate determinations of fundamental stellar parameters (in particular, masses) for input to models of stellar evolution, which are poorly constrained in this age range. We defer discussion of our eclipsing binary candidates to a later paper once we have obtained suitable follow-up spectroscopy.

These observations are part of a larger photometric monitoring survey of young open clusters over a range of ages and metalicities (the Monitor project; Hodgkin et al. 2006; Aigrain et al. 2007).

The remainder of the paper is structured as follows. The observations and data reduction are described in Section 2, and the colour–magnitude diagram (CMD) of the cluster and candidate membership selection are presented in Section 3. The method we use for obtaining photometric periods is summarized in Section 4 (see Irwin et al. 2006 for a more detailed discussion), and our results are summarized in Section 5. We discuss the implications of these results in Section 6, and our conclusions are summarized in Section 7.

2 OBSERVATIONS AND DATA REDUCTION

Photometric monitoring observations were obtained using the MPG/ESO 2.2-m telescope with WFI in service mode, with ~100 h

of observations distributed over a ~8 month period from 2005 October to 2006 May. The instrument provides a field of view (FOV) of ~34 × 33 arcmin^2 (0.31 deg^2), using a mosaic of eight 2k × 4k pixel CCDs, at a scale of ~0.238 arcsec pix^{-1}.

In order to maximize the number of cluster members covered by our survey we elected to use two fields, with a 120 s *I*-band exposure in each, observed by cycling between them, to give a cadence of ~7 min, covering ~0.6 deg^2 of the cluster, illustrated in Fig. 1. Our observations are sufficient to give 1 per cent or better photometric precision per data point from saturation at $I \sim 14$ down to $I \sim 18$ (see Fig. 2), covering K to mid M spectral types at the age and distance of NGC 2547.

We also obtained 120 and 1500 s *V*-band exposures in each field during photometric conditions, to generate a CMD.

For a full description of our data reduction steps, the reader is referred to Irwin et al. (2007a). Briefly, we used the pipeline for
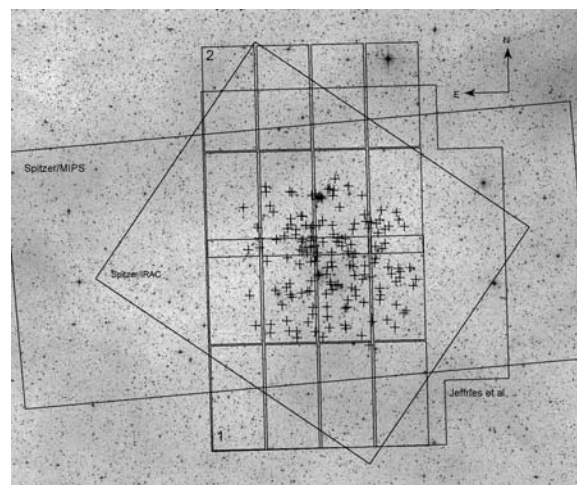

Figure 1. Digitized sky survey image of NGC 2547 covering ~1°4 × 1°3, showing the coverage of the present survey (numbered eight-chip mosaic tiles), the *Spitzer* IRAC and MIPS fields of Young et al. (2004), and the optical survey of Jeffries et al. (2004). Crosses show the positions of the X-ray sources from Jeffries et al. (2006).
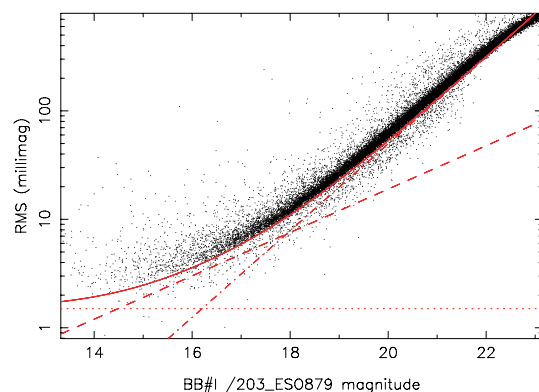

Figure 2. Plot of rms scatter as a function of magnitude for the *I*-band observations of a single field in NGC 2547, for all unblended objects with stellar morphological classifications. The diagonal dashed line shows the expected rms from Poisson noise in the object, the diagonal dot–dashed line shows the rms from sky noise in the photometric aperture, and the dotted line shows an additional 1.5 mmag contribution added in quadrature to account for systematic effects. The solid line shows the overall predicted rms, combining these contributions.

the INT wide-field survey (Irwin & Lewis 2001) for 2D instrumental signature removal (bias correction, flat-fielding, defringing) and astrometric and photometric calibration. We then generated a master catalogue for each filter by stacking 20 of the frames taken in the best conditions (seeing, sky brightness and transparency) and running the source detection software on the stacked image. The resulting source positions were used to perform aperture photometry on all of the time-series images. We achieved a per data point photometric precision of ∼2–4 mmag for the brightest objects, with rms scatter <1 per cent for $I \lesssim 18$ (see Fig. 2).

Our source detection software flags any objects detected as having overlapping isophotes. This information is used, in conjunction with a morphological image classification flag also generated by the pipeline software (Irwin & Lewis 2001) to allow us to identify non-stellar or blended objects in the time-series photometry.

Photometric calibration of our data was carried out using regular observations of Landolt (1992) equatorial standard star fields in the usual way, as part of the standard ESO nightly calibrations.

Light curves were extracted from the data for ∼130 000 objects, 90 000 of which had stellar morphological classifications, using our standard aperture photometry techniques, described in Irwin et al. (2007a). We fit a 2D quadratic polynomial to the residuals in each frame (measured for each object as the difference between its magnitude on the frame in question and the median calculated across all frames) as a function of position, for each of the eight CCDs separately. Subsequent removal of this function accounted for effects such as varying differential atmospheric extinction across each frame. Over a single CCD, the spatially varying part of the correction remains small, typically ∼0.02 mag peak to peak. The reasons for using this technique are discussed in more detail in Irwin et al. (2007a).

For the production of deep CMDs, we used the *I*-band master catalogue, and combined the *V*-band exposures. The limiting magnitudes, measured as the approximate magnitude at which our catalogues are 50 per cent complete on these images were $V \sim 23$ and $I \sim 23$.

3 SELECTION OF CANDIDATE LOW-MASS MEMBERS

A catalogue of photometrically selected candidate members (using *R I Z* photometry) covering most of our survey area was available from Jeffries et al. (2004) for solar mass down to ∼0.05 M$_\odot$ (limiting magnitude $I \simeq 19.5$), but we elected to perform a new photometric selection using *V* versus $V - I$ CMDs from our data, to make better use of the deeper limiting magnitudes of the present survey.

3.1 The *V* versus $V - I$ CMD

Our CMD of NGC 2547 is shown in Fig. 3. The *V* and *I* measurements were converted to the standard Johnson–Cousins photometric system using colour equations derived from standard star observations by Mike Irwin (private communication):

$$(V - I) = (V_{\text{ccd}} - I_{\text{ccd}})/1.14, \tag{1}$$

$$V = V_{\text{ccd}} - 0.08(V - I), \tag{2}$$

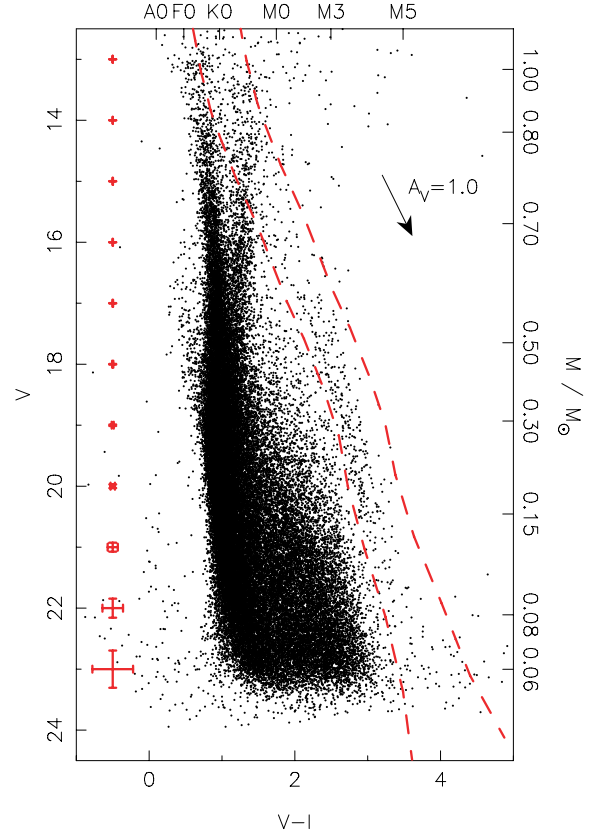$$I = I_{\text{ccd}} + 0.06(V - I). \tag{3}$$

Figure 3. *V* versus $V - I$ CMD of NGC 2547 from stacked images, for all objects with stellar morphological classification. The cluster sequence is clearly visible on the right-hand side of the diagram. The boundaries of the region used to select photometric candidate members are shown by the dashed lines (all objects between the dashed lines were selected). The reddening vector for $A_V = 1.0$ is shown at the right-hand side of the diagram. The mass scale is from the 40 Myr NextGen models (Baraffe et al. 1998) for $M > 0.1$ M$_\odot$, and the 50 Myr DUSTY models (Chabrier et al. 2000) for $M < 0.1$ M$_\odot$, using our empirical isochrone to convert the *V* magnitudes to *I* magnitudes, and subsequently obtaining the masses from these, due to known problems with the *V* magnitudes from the models (see Section 3.1). The error bars at the left-hand side of the plot indicate the typical photometric error for an object on the cluster sequence.

Candidate cluster members were selected by defining an empirical cluster sequence 'by eye' to follow the clearly visible cluster single-star sequence. The cuts were defined by moving this line along a vector perpendicular to the cluster sequence, by amounts $k - \sigma(V - I)$ and $k + \sigma(V - I)$ as measured along this vector, where $\sigma(V - I)$ is the photometric error in the $V - I$ colour. The values of k used were −0.15 mag for the lower line and 0.5 mag for the upper line on the diagram, making the brighter region wider to avoid rejecting binary and multiple systems, which are overluminous for their colour compared to single stars. 800 candidate photometric members were selected, over the full *V* magnitude range from $V = 12.5$ to 24, but the well-defined cluster sequence appears to terminate at $M \sim 0.1$ M$_\odot$, or $V \sim 21$, with a few candidate members below this limit, but with high field contamination.

The selection region used here is comparable to that of Jeffries et al. (2004), and below $V \sim 16$, 100 per cent of their candidate

cluster members are also selected by our cut. Above $V \sim 16$, there are slight differences in the isochrones and due to saturation in the present sample, and the corresponding fraction is reduced to $\sim$90 per cent.

We also considered using the model isochrones of Baraffe et al. (1998) and Chabrier et al. (2000) for selecting candidate members. The NextGen model isochrones were found to be unsuitable due to the known discrepancy between these models and observations in the $V - I$ colour for $T_{eff} \lesssim 3700$ K (corresponding here to $V - I \gtrsim 2$). This was examined in more detail by Baraffe et al. (1998), and is due to a missing source of opacity at these temperatures, leading to overestimation of the V-band flux. Consequently, when we have used the NextGen isochrones to determine model masses and radii for our objects, the I-band absolute magnitudes were used to perform the relevant look-up, since these are less susceptible to the missing source of opacity, and hence give more robust estimates.

3.2 Contamination

In order to estimate the level of contamination in our catalogue, we used the Besançon Galactic models (Robin et al. 2003) to generate a simulated catalogue of objects passing our selection criteria at the Galactic coordinates of NGC 2547 ($l = 264°.4$, $b = -8°.5$), covering the total FOV of $\sim$0.59 deg^2 (including gaps between detectors). We selected all objects over the apparent magnitude range $10 < V < 24$, giving 120 000 stars. The same selection process as above for the cluster members was then applied to find the contaminant objects. A total of 888 simulated objects passed these membership selection criteria, giving an overall contamination level of $\sim$59 per cent after correcting for bins where the number of objects predicted by the models exceeded the number actually observed (we simply assumed 100 per cent field contamination in these bins). Fig. 4 shows the contamination as a function of V magnitude. We note that this figure is somewhat uncertain due to the need to use Galactic models, and especially given the overestimation of the numbers of observed objects by the models. Follow-up data will be required to make a more accurate estimate.
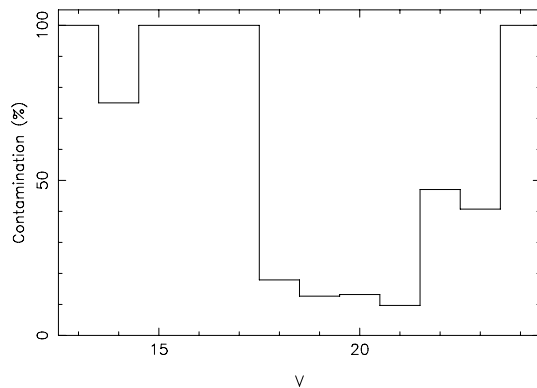

Figure 4. Contamination, measured as the ratio of the calculated number of objects in each magnitude bin from the Galactic models, to the number of objects detected and classified as candidate cluster members in that magnitude bin. Note that bins with contamination estimates >100 per cent (where there were more objects in that bin from the Galactic model than were actually observed) have been truncated to 100 per cent.

4 PERIOD DETECTION

4.1 Method

The method we use for detection of periodic variables is described in detail in Irwin et al. (2006), and we provide only a brief summary here. The method uses least-squares fitting of sine curves to the time-series $m(t)$ (in mag) for *all* candidate cluster members, using the form

$$m(t) = m_{dc} + \alpha \sin(\omega t + \phi), \tag{4}$$

where m_{dc} (the DC light curve level), α (the amplitude) and ϕ (the phase) are free parameters at each value of ω over an equally spaced grid of frequencies, corresponding to periods from 0.005 to 100 d for the present data set.

Periodic variable light curves were selected by evaluating the change in reduced χ^2:

$$\Delta \chi_\nu^2 = \chi_\nu^2 - \chi_{\nu,smooth}^2 > 0.4, \tag{5}$$

where χ_ν^2 is the reduced χ^2 of the original light curve with respect to a constant model, and $\chi_{\nu,smooth}^2$ is the reduced χ^2 of the light curve with the smoothed, phase-folded version subtracted. This threshold was used for the M34 data and appears to work well here too, carefully checked by examining all the light curves for two of the detectors, chosen randomly. A total of 482 objects were selected by this automated part of the procedure.

The selected light curves were examined by eye, to define the final sample of periodic variables. A total of 176 light curves were selected, with the remainder appearing non-variable or too ambiguous to be included.

4.2 Simulations

Monte Carlo simulations were performed following the method detailed in Irwin et al. (2006), injecting simulated signals of 2 per cent amplitude and periods chosen following a uniform distribution on $\log_{10}$ period from 0.1 to 20 d, into light curves covering a uniform distribution in mass, from 1.0 to 0.1 M$_\odot$. A total of 1015 objects were simulated.

The results of the simulations are shown in Fig. 5 as diagrams of completeness, reliability and contamination as a function of period and stellar mass. Broadly, our period detections are close to 100 per cent complete from 0.9 to 0.1 M$_\odot$, with remarkably little period dependence. Fig. 6 shows a comparison of the detected periods with real periods for our simulated objects, indicating remarkably high reliability, especially compared to the earlier data sets (Irwin et al. 2006, 2007b), resulting from the extremely long time baseline of the present survey afforded by observing in service mode.

These results indicate overall that the service mode observing strategy as implemented by ESO performs very favourably for rotation period detection in NGC 2547, compared to our conventional visitor mode observations (e.g. Irwin et al. 2006, 2007b). In particular, the sampling is very well suited to determining extremely precise and accurate rotation periods, as illustrated in Fig. 6.

However, there are two principal disadvantages. The long time-span of the observations, and sparse sampling, here over $\sim$8 months, means the process of period detection is complicated by the evolution of the spot patterns on the stellar surfaces giving rise to the photometric modulations. This has the effect of modifying the amplitude and phase of the variability, and may occur over time-scales of a few months. This has not been accounted for in the simulations. Qualitatively, this effect may reduce the overall detection
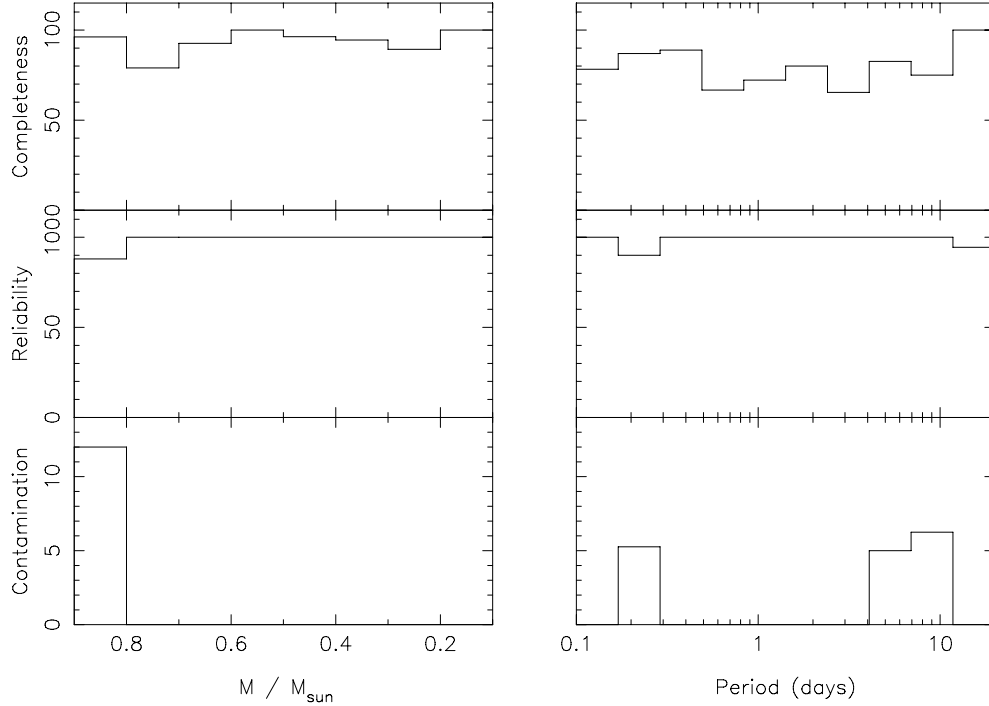
Figure 5. Results of the simulations for 0.02 mag amplitude expressed as percentages, plotted as a function of mass (left-hand panel) and period (right-hand panel). The simulated region covered $0.1 < M/M_\odot < 0.9$ in order to be consistent with the NGC 2547 sample. Top panels: completeness as a function of real (input) period. Central panels: Reliability of period determination, plotted as the fraction of objects with a given true period, detected with the correct period (defined as differing by < 20 per cent from the true period). Bottom panels: Contamination, plotted as the fraction of objects with a given detected period, having a true period differing by >20 per cent from the detected value.
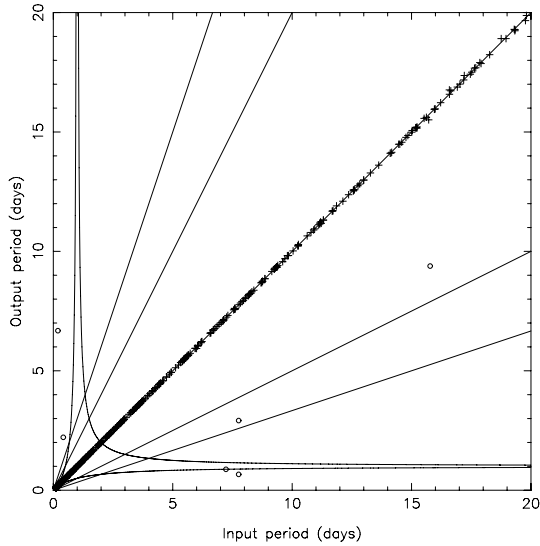

Figure 6. Detected period as a function of actual (input) period for our simulations. Objects plotted with crosses had fractional period error <10 per cent, open circles >10 per cent. The straight lines represent equal input and output periods, and factors of 2, 3, 1/2 and 1/3. The curved lines are the loci of the $\pm 1\,\mathrm{d}^{-1}$ aliases resulting from gaps during the day. The majority of the points fall on (or close to) the line of equal periods.

rate since the variations will not produce a smooth phase-folded light curve for any plausible period, and will therefore be rejected in the detection process. Furthermore, for eclipsing binary detection this is obviously a serious problem, since the variations be-

come much more difficult to remove when searching for shallow eclipses.

The second problem relates to the observing conditions. Since desired weather conditions are specified for a service mode proposal, and differential photometry does not require the best observing conditions, a service mode programme will in general receive poorer conditions than a visitor mode programme performed in good weather (e.g. the NGC 2516 survey; Irwin et al. 2007b). For rotation period detection at reasonable amplitudes, the simulations indicate that this is not a serious issue. However, poor seeing and particularly poor transparency, increase the level of low-amplitude-correlated noise in the light curves (see Irwin et al. 2007a), which severely impedes detection of shallow transit events.

The effects of both these factors on transit detection will be evaluated in more detail in a future publication presenting our eclipse candidates.

4.3 Detection rate and reliability

The locations of our detected periodic variable candidate cluster members on a V versus $V - I$ CMD of NGC 2547 are shown in Fig. 7. The diagram indicates that the majority of the detections lie on the single-star cluster sequence, as would be expected for rotation in cluster stars as opposed to, say, eclipsing binaries.

Fig. 8 shows the fraction of cluster members with detected periods as a function of V magnitude. The decaying parts of the histogram at the bright and faint ends may be caused by the increased field contamination here (see Fig. 4), since we expect field objects on average show less rotational modulation than cluster objects, incompleteness effects resulting from saturation for $V \lesssim 14$, and for
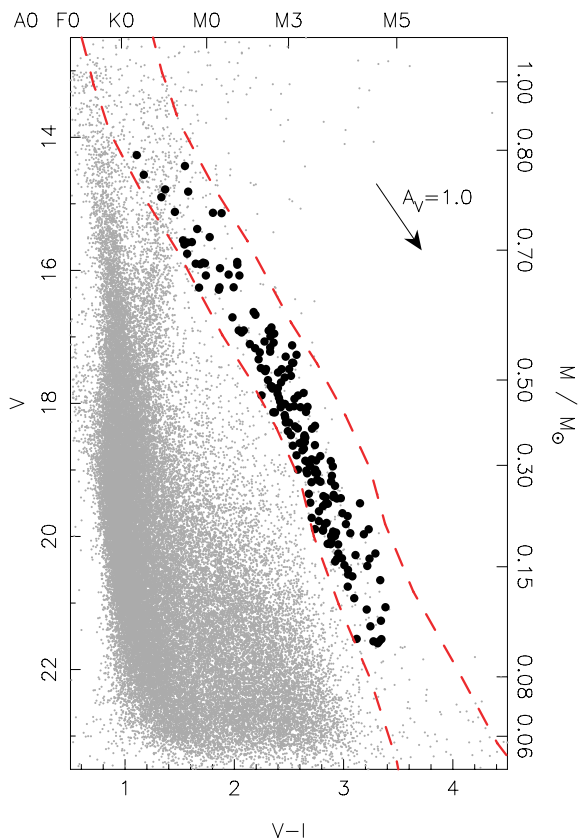
et al. 2007b), and the three distributions look qualitatively very similar after correcting for the different mass ranges covered, with a rise in the fraction of periodic objects detected at spectral types of $\sim$ M0. However, in all three cases, this is also the point at which the cluster sequence becomes well separated from the field in the CMD analysis, corresponding to a reduction in field contamination moving towards later spectral types. It is therefore difficult to say if the trend is significant from the present observations.

Likewise, lower field contamination is expected in the rotation sample than in the full candidate membership sample. Typical field population ages for the young disc of 3 Gyr (Mayor 1974; Meusinger, Stecklum & Reimann 1991) imply slower rotation rates by factors of $\sim$ a few than cluster members, and reduced activity, implying smaller asymmetric components of the spot coverage and hence lower photometric amplitudes (which probably render many of them undetectable).

The properties of all our rotation candidates are listed in Table 1.

4.4 Non-periodic objects

The population of objects rejected by the period detection procedure described in Section 4 was examined, finding that the most variable population of these light curves (which might correspond to non-periodic or semi-periodic variability) was contaminated by a small number of light curves ($\sim$50) exhibiting various uncorrected systematic effects, mostly seeing-correlated variations due to image blending. It is therefore difficult to quantify the level of non-periodic or semi-periodic variability in NGC 2547 from our data. Qualitatively however, there appear to be very few of these variables, and examining the light curves indicated only $\sim$10 obvious cases, some of which resembled eclipses (presumably due to eclipsing binaries), and will be the subject of a later Monitor project paper.

5 RESULTS

5.1 NGC 2547 rotation periods

Plots of period as a function of $V - I$ colour and mass for the objects photometrically selected as possible cluster members are shown in Fig. 9. These diagrams show a striking correlation between stellar mass (or spectral type) and the longest rotation period seen at that mass, with a clear lack of slow rotators at very low masses. This trend is also followed by the majority of the rotators, with only a tail of faster rotators to $\sim$0.2 d periods. Furthermore, very few objects were found rotating faster than this, implying a hard lower limit to the observed rotation periods at 0.2 d.

Could the apparent morphology in Fig. 9 be explained by sample biases? The simulations of Section 4.2 suggest that this is unlikely, since we are sensitive to shorter periods than the 0.2–0.3 d 'limit', and the slight bias towards detection of shorter periods at low mass is not sufficient to explain the observations for the slow rotators. Furthermore, Fig. 10 indicates that the lack of sensitivity to low amplitudes at low masses does not appear to introduce any systematic changes in the detected periods.

Fig. 10 shows an apparent lack of objects with masses $M < 0.4 \, M_\odot$ and rotation periods $\gtrsim$2 d, a region of the diagram where the survey is sensitive down to amplitudes of 0.01 mag (see also Section 4.2).

A very large fraction ($\sim$50 per cent) of the bright rotators ($M \gtrsim 0.4 \, M_\odot$) were detected in the X-ray survey of Jeffries et al. (2006). Detection in X-rays is suggestive of youth and hence cluster membership, which confirms that the level of field contamination is

Figure 7. Magnified *V* versus *V − I* CMD of NGC 2547, for objects with stellar morphological classification, as Fig. 3, showing all 176 candidate cluster members with detected periods (black points). The dashed lines show the cuts used to select candidate cluster members (see Section 3.1).
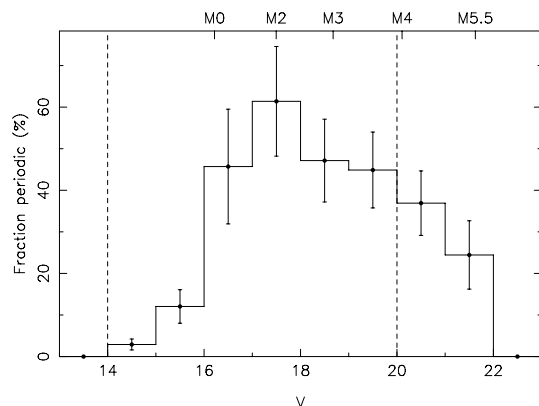

Figure 8. Fraction of candidate cluster members detected as periodic variables, plotted as a function of magnitude. This distribution has not been corrected for incompleteness in the period detections, which are close to 100 per cent complete for $14 < V < 20$ (shown by the vertical dashed lines), or for the effects of field contamination.

$V \gtrsim 20$, the gradual increase in the minimum amplitude of variations we can detect (corresponding to the reduction in sensitivity moving to fainter stars, see Fig. 2).

In the M34 survey of Irwin et al. (2006), we commented on a possible increase in the fraction of photometric variables from *K* to *M* spectral types, subject to a large uncertainty due to small number statistics. This feature was also seen in the NGC 2516 survey (Irwin

Table 1. Properties of our 176 rotation candidates. The period *P* in days, *i*-band amplitude α_i (units of magnitudes, in the instrumental bandpass), interpolated mass and radius (from the models of Baraffe et al. 1998, derived using the *I* magnitudes) are given (where available). Our identifiers are formed using a simple scheme of the cluster name, field number, CCD number and a running count of stars in each CCD, concatenated with dashes. The full table is available in the electronic edition (see supplementary material section of this article). Machine-readable copies of the data tables from all the Monitor rotation period publications are also available at http://www.ast.cam.ac.uk/research/monitor/rotation/.

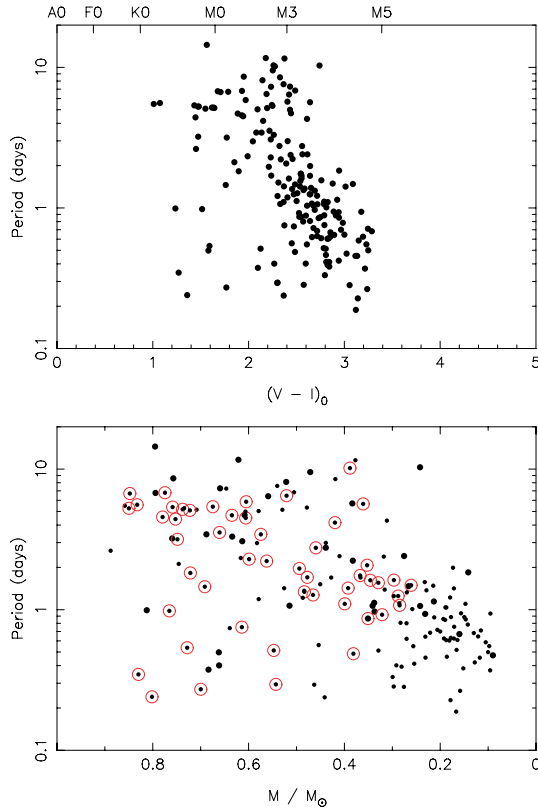| Identifier	RA J2000	Dec. J2000	*V* (mag)	*I* (mag)	*P* (d)	α_i (mag)	*M* (M$_\odot$)	*R* (R$_\odot$)
N2547-1-1-2501	08 11 20.69	−48 49 22.5	17.97	15.55	2.758	0.014	0.44	0.56
N2547-1-1-3141	08 11 32.39	−48 48 01.0	17.78	15.43	9.523	0.009	0.47	0.59
N2547-1-1-3640	08 11 59.66	−48 46 56.8	15.58	14.01	3.213	0.038	0.76	0.82
N2547-1-1-3903	08 11 22.55	−48 46 29.8	14.90	13.57	0.991	0.005	0.81	0.89
N2547-1-1-4637	08 11 46.91	−48 44 54.0	17.16	14.83	3.071	0.024	0.61	0.69

Figure 9. Plots of rotation period as a function of dereddened *V − I* colour (top), and mass (bottom) for NGC 2547, deriving the masses using the 40 Myr NextGen mass–magnitude relations of Baraffe et al. (1998) and the measured *I*-band magnitudes.

Figure 10. Plots of amplitude as a function of period for NGC 2547, in two mass bins: $0.4 \leqslant M/M_\odot < 1.0$ (top) and $M < 0.4\,M_\odot$ (bottom).

low in the rotation sample, especially when the incomplete spatial overlap between our optical survey and the *XMM–Newton* observation of Jeffries et al. (2006) is accounted for. Very few of the lower mass stars in Fig. 9 were detected in X-rays (e.g. for $M < 0.3\,M_\odot$ there was only a single X-ray detection), but this is not surprising since these objects are fainter. Indeed, fig. 3 of Jeffries et al. (2006) indicates that the X-ray detection limit for a cluster member corresponds to $I \sim 16$, equivalent to $M \sim 0.34\,M_\odot$ with the models we are using.

5.1.1 Period distributions

In order to quantify the morphology of Fig. 9, we have used histograms of the rotation period distributions in two broad mass bins,
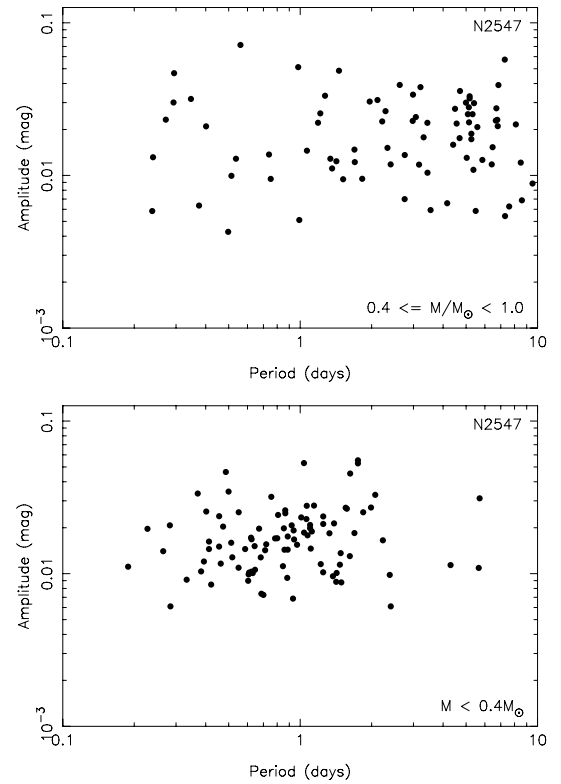
$0.4 \leqslant M/M_\odot < 1.0$ and $M < 0.4\,M_\odot$, shown in Fig. 11. We have attempted to correct the distributions for the effects of incompleteness and (un)reliability using the simulations described in Section 4.2, following the method used in Irwin et al. (2006). The results of doing this are shown in the solid histograms in Fig. 11, and the raw period distributions in the dashed histograms.

The period distributions in the two mass bins of Fig. 11 show clear differences, with the low-mass stars ($M < 0.4\,M_\odot$) showing a strongly peaked rotational period distribution, with a maximum at $\sim$0.6–0.7 d, whereas the higher mass stars ($0.4 \leqslant M/M_\odot < 1.0$) show a broader distribution. We applied a two-sided Kolmogorov–Smirnov test to the corrected distributions to confirm the statistical significance of this result, finding a probability of 2×10^{-13} that the distributions were drawn from the same parent population.
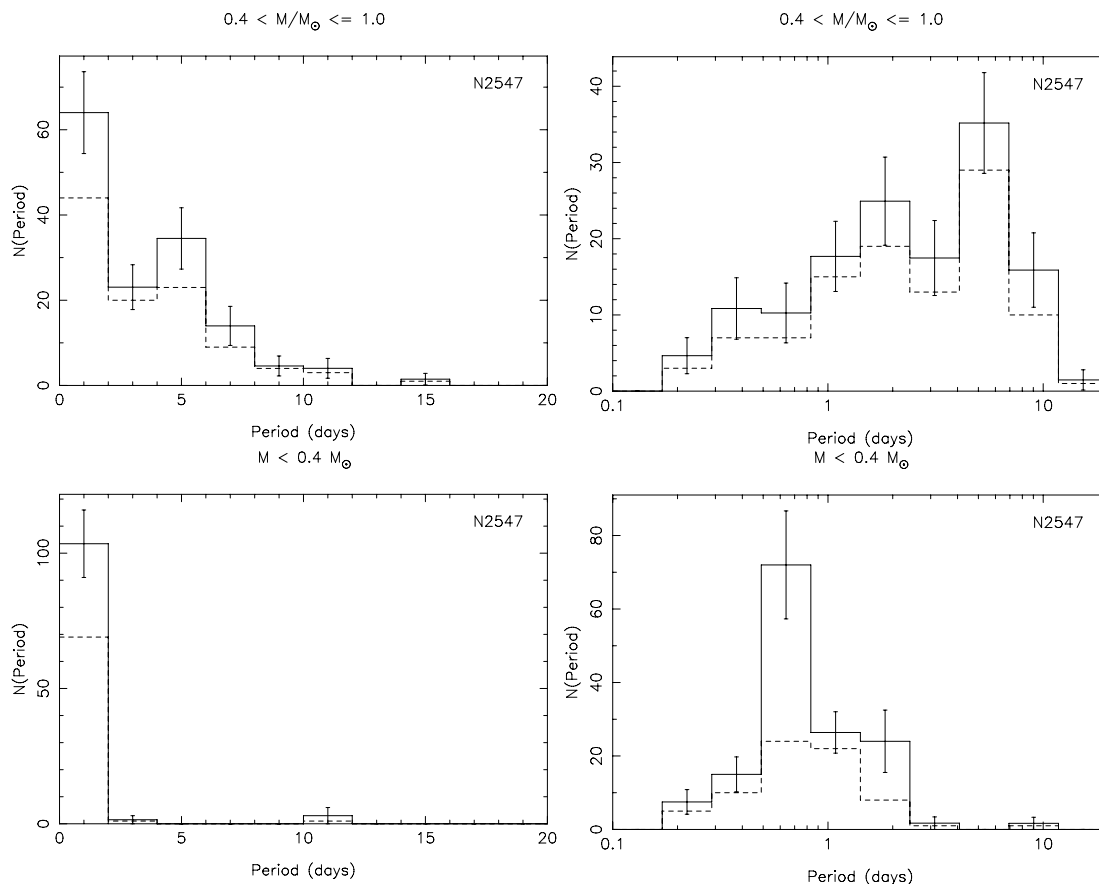
Figure 11. Period distributions for objects classified as possible photometric members, in two mass bins: $0.4 \leqslant M/M_\odot < 1.0$ (upper row, corresponding roughly to K and early-M spectral types) and $M < 0.4\,M_\odot$ (lower row, late-M). The left-hand panels show the distributions plotted in linear period, and the right-hand panels show the same distributions plotted in $\log_{10}$ period. The dashed lines show the measured period distributions, and the solid lines show the results of attempting to correct for incompleteness and reliability, as described in the text.

The implication of this result is that the observed morphology in Fig. 9, and in particular the increase of the longest observed rotation period as a function of increasing mass, a trend followed also by the bulk of the rotators, is real and statistically significant.

5.1.2 Rapid rotators

We have examined the periods of our fastest rotating stars, to check if they are rotating close to their break-up velocity. The critical period P_{crit} for break-up is given approximately by

$$P_{crit} = 0.116 \frac{(R/R_\odot)^{3/2}}{(M/M_\odot)^{1/2}}\,d, \tag{6}$$

where R and M are the stellar radius and mass, respectively (e.g. Herbst et al. 2002). Using the NextGen models of Baraffe et al. (1998), the object rotating closest to break-up is N2547-2-2-1563, with $P_{crit}/P = 0.46$. However, the majority of our objects are rotating at much lower fractions of their break-up velocity.

Fig. 10 indicates that there is only one object with $P < 0.2\,d$, N2547-2-2-1485 at $P = 0.188\,d$. Therefore, in common with the other clusters we have studied, we find a short-period limit of ~ 0.15–$0.2\,d$, with no objects found rotating faster than this rate.

5.2 The rotation–activity relation

Observations of open clusters in the age range 50 Myr to several Gyr have established an age–rotation–activity relationship, where younger stars tend to be more rapidly rotating, and emit strong X-rays (up to a saturation level), whereas older stars have spun down to lower rotation rates, and emit a smaller fraction of their flux in X-rays (Jeffries 1999; Randich 2000). Jeffries et al. (2006) established that G and K stars in NGC 2547 follow the same relationship between X-ray activity and Rossby number established for field stars and old clusters, but at saturated or supersaturated X-ray activity levels, with L_X/L_{bol} values similar to those for T-Tauri stars in the ONC, but an order of magnitude higher than in the Pleiades. In this section, we re-evaluate the rotation–activity relation using the present NGC 2547 rotation period sample, which probes to lower masses than the sample of Jeffries et al. (2006).

Following the method of Jeffries et al. (2006), Fig. 12 shows a plot of X-ray activity as a function of the Rossby number, defined as the ratio of rotation period to convective overturn time-scale at the base of the convection zone, τ_{conv}. Our X-ray luminosities were taken from Jeffries et al. (2006), but assuming a distance of 361 pc for consistency with the distance modulus of 7.79 we assume in this work (see Section 1). Bolometric luminosities were calculated from
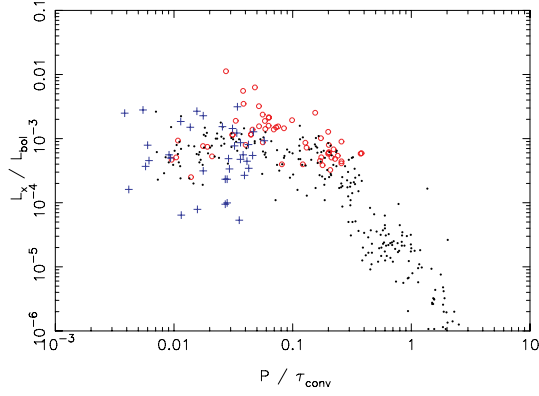
Figure 12. Plot of X-ray activity (0.1–2.4 keV luminosity divided by bolometric luminosity, as Jeffries et al. 2006) as a function of the Rossby number for the NGC 2547 rotation period data (open circles). Also shown are the compilation of results for field and cluster stars (small black points) from Pizzolato et al. (2003), and for ONC stars in the range $0.5 < M/M_\odot < 1.2$ (crosses) from Getman et al. (2005), assuming a fixed value of $\tau_c = 250$ yr (see Preibisch et al. 2005; Jeffries et al. 2006).

the V-band absolute magnitudes and $V − I$ colours using a quadratic fit to the empirical bolometric corrections and colours of Leggett et al. (1996):

$$\mathrm{BC}_V = 0.243 - 0.583(V - I) - 0.128(V - I)^2. \tag{7}$$

The values of τ_{conv} were derived using equation (4) of Noyes et al. (1984) and $B − V$ colours of our stars, obtained from a linear fit to the intrinsic stellar colours of Leggett (1992):

$$(B - V) = 0.907 + 0.268(V - I). \tag{8}$$

These relations should give reliable results over the entire late-K to mid-M range of spectral types covered by the present rotation sample.

Comparing Fig. 12 to fig. 9 of Jeffries et al. (2006) shows that we reproduce the same trend of X-ray activity with Rossby number seen in the earlier NGC 2547 work, and the ONC, where we have used a similar plot scale to aid comparison with their figure.

A small group of objects at $P/\tau_{\mathrm{conv}} \lesssim 0.025$ and $L_X/L_{\mathrm{bol}} \sim 10^{-3}$ in the NGC 2547 sample have unusually small values of P/τ_{conv} compared to the remainder of the NGC 2547 objects. These all have very short rotation periods ($\lesssim 0.6$ d). Comparing with fig. 9 of Jeffries et al. (2006) indicates that they also see one object in this region of the diagram. It is possible that these objects could show fast rotation rates as a result of tidal synchronization effects in binary systems, a hypothesis which could be verified with follow-up spectroscopy.

There are also a small number of objects showing unusually strong X-ray emission, with L_X/L_{bol} values up to $\sim 10^{-2}$, which were not seen by Jeffries et al. (2006). Such high X-ray luminosities would be indicative of very strong activity, or alternatively, overestimation of L_X or underestimation of L_{bol}. These objects could also result from misidentification of a very luminous background AGN in X-rays with a cluster star in the optical, given the large search radii (here 6 arcsec) which must be used due to the limited astrometric accuracy of the X-ray data.

In order to attempt to trace the rotation–activity relation to lower mass in NGC 2547, it would be desirable to obtain deeper X-ray observations, since the stars with masses $\lesssim 0.35 M_\odot$ were
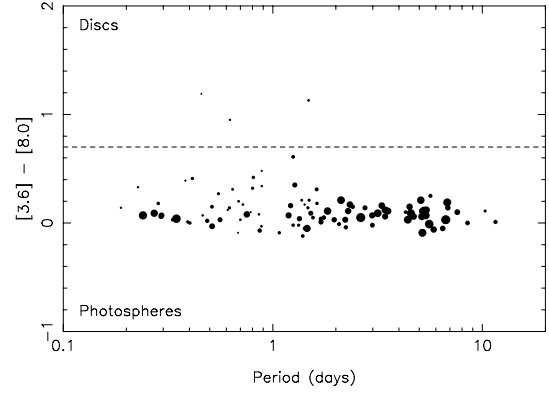

Figure 13. Plot of [3.6]–[8.0] colour as a function of period. The sizes of the symbols indicate the masses of the objects, with the smallest symbols corresponding to $M \sim 0.1 M_\odot$, and the largest to $M \sim 0.9 M_\odot$. The horizontal dashed line indicates the threshold of [3.6]–[8.0] > 0.7 used by Cieza & Baliber (2006) to select objects showing 8.0 μm excesses.

not detected in the existing *XMM–Newton* observations of Jeffries et al. (2006).

5.3 Comparison with mid-IR *Spitzer* observations

We have compared the rotation period results to the mid-IR *Spitzer* observations of Gorlova et al. (2007), to search for any correlation between mid-IR excess (presumably due to a circumstellar disc) and rotation period, as would be expected in the disc regulation paradigm for angular momentum evolution on the early pre-main sequence (PMS).

Fig. 13 shows a plot of [3.6]–[8.0] colour versus rotation period. There are only three objects in the rotation period sample identified as having possible 8.0 μm excesses. These are N2547-1-6-3669, N2547-2-2-6311, and N2547-2-3-6494. Of these, the latter two objects are flagged by Gorlova et al. (2007) as having possibly unreliable 8.0 μm measurements, due to the presence of nearby sources or other image features which might contribute to the measured flux (confirmed by visual examination of our *I*-band images). Therefore, only one object, N2547-1-6-3669, has a reasonably reliable 8.0 μm excess. This has a very low inferred mass of 0.21 $M_\odot$, and falls on the locus of slow rotators at this mass, having a rotation period of 1.48 d.

Given the extremely small number of objects under discussion, it is difficult to draw any conclusions regarding the disc regulation paradigm. However, the only object with reliable evidence of an inner disc, N2547-1-6-3669, is indeed a slow rotator, as would be expected if its angular velocity was regulated by the presence of the disc.

One object in the rotation sample has a 24 μm detection, and shows an excess in this band: N2547-1-5-1123. Again, this has a low inferred mass of 0.25 $M_\odot$, but is a rapid rotator, having a period of 0.41 d. This object does not have an 8 μm excess, indicating that the inner disc has cleared, which may also be consistent with the disc regulation paradigm, since the inner disc is most likely the part that couples to the star to induce angular momentum loss and prevent it from spinning up.

The existence of a relatively large fraction of 24 μm detections in the sample of Gorlova et al. (2007) motivates deeper MIPS observations, to probe to lower masses: the existing observations were only sufficient to detect photospheres down to F spectral types. The

single object with a 24 μm detection has a mid-M spectral type, and was only detected as a result of its large 24 μm excess.

5.4 Comparison with other data sets

5.4.1 Period versus mass diagram

Fig. 14 shows a diagram of rotation period as a function of stellar mass for the ONC (1 ± 1 Myr; Hillenbrand 1997), NGC 2264 (2–4 Myr; Park et al. 2000), NGC 2362 (~5 ± 1 Myr; Balona & Laney 1996; Moitinho et al. 2001), NGC 2547, the Pleiades (~100 Myr; Meynet, Mermilliod & Maeder 1993), NGC 2516 (~150 Myr; Jeffries, Thurston & Hambly 2001) and M34 (~200 Myr; Jones & Prosser 1996). Data sources for each cluster are indicated in the figure caption.

The diagram clearly shows a gradual evolutionary sequence, from a relatively flat mass dependence of the rotation periods in the ONC (~1 Myr), to a sloping relation in NGC 2362 (~5 Myr) and NGC 2547, and the emergence of the break between a flat distribution for $M \gtrsim 0.6\,M_\odot$ and strongly sloping distribution at lower masses, for the Pleiades, NGC 2516 (~150 Myr) and M34 (~200 Myr), as discussed in Irwin et al. (2007b).

6 DISCUSSION

6.1 Link to angular momentum

It is instructive to re-examine Fig. 9 in terms of the stellar angular momentum J. We define

$$J = I\omega \tag{9}$$

$$= \frac{2\pi k^2 M R^2}{P}, \tag{10}$$

where $I = k^2 M R^2$ is the moment of inertia of a star of mass M and radius R, k is the radius of gyration ($k^2 = 2/5$ for a uniform sphere rotating as a solid body), and $\omega = 2\pi/P$ is the rotational angular velocity. A plot of J as a function of stellar mass for the NGC 2547 sample is shown in Fig. 15.

We computed the median angular momentum as a function of mass for the NGC 2547 data, shown in Fig. 15. The relation is consistent with the same $J \propto M$, or specific angular momentum $j = $ constant, relation as seen by Irwin et al. (2007b), and consistent with the conclusions of Herbst, Bailer-Jones & Mundt (2001) in the ONC. The lack of any change in the median relation for stars still undergoing contraction on the PMS indicates that any mass-dependent angular momentum losses are not important in determining the evolution of the median over this age range, unless high angular momentum is hidden in a fast rotating radiative core. However, this is not the case in detail or once the stars reach the ZAMS, in particular it is clear (e.g. from Fig. 14) the *shape* of the distribution does evolve in a mass-dependent fashion (see also the next section).

6.2 Simple models

6.2.1 Description

For a full description of our simple model scheme, the reader is referred to the NGC 2516 publication (Irwin et al. 2007b). Briefly, we have generated models for solid body rotation, and a simple implementation of core-envelope decoupling where the core and
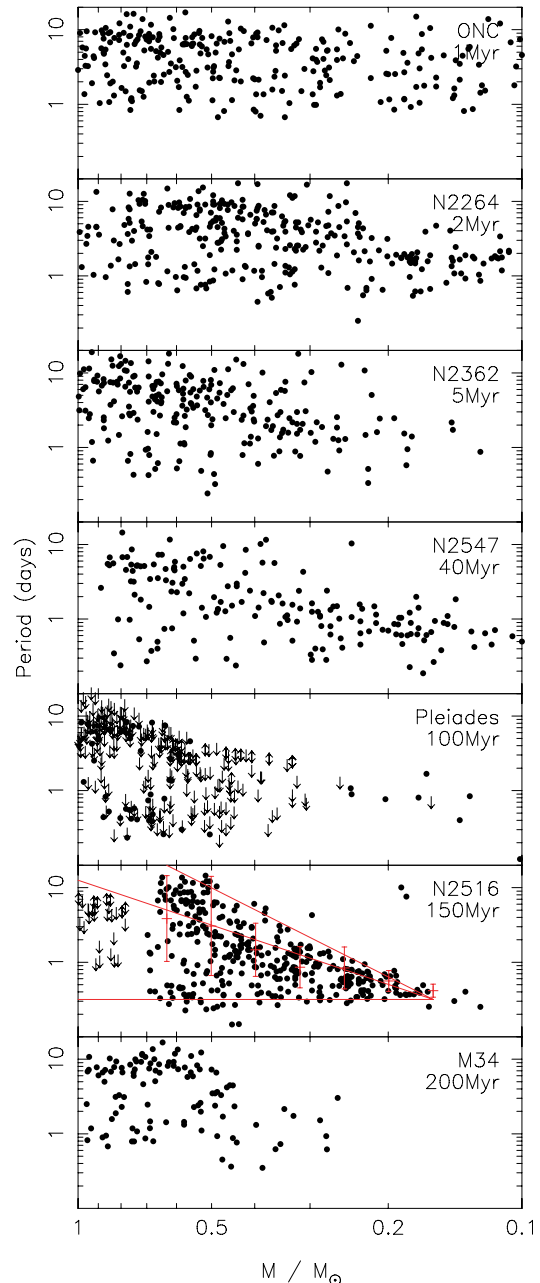

Figure 14. Rotation period as a function of stellar mass for (top to bottom): ONC, NGC 2264, 2362, 2547, the Pleiades, NGC 2516 and M34. Lower and upper limits (from $v \sin i$ data) are marked with arrows. The masses were taken from the NextGen mass–magnitude relations (Baraffe et al. 1998) at the appropriate ages. The ONC data are from Herbst et al. (2002). For NGC 2264 we used the data of Lamm et al. (2005) and Makidon et al. (2004). The NGC 2362 data are from the Monitor project, to be published in Irwin et al. (2007c). The Pleiades rotation period data are a compilation of the results from Van Leeuwen, Alphenaar & Meys (1987), Stauffer et al. (1987), Magnitskii (1987), Prosser et al. (1993a,b, 1995), Krishnamurthi et al. (1998) (taken from the open cluster data base), Terndrup et al. (1999) and Scholz & Eislöffel (2004). The Pleiades $v \sin i$ data are a compilation of results from Stauffer et al. (1984), Stauffer & Hartmann (1987), Soderblom et al. (1993), Jones, Fischer & Stauffer (1996), Queloz et al. (1998) and Terndrup et al. (2000). The NGC 2516 data are taken from Irwin et al. (2007b), plus upper limits from Terndrup et al. (2002), and the M34 data from Irwin et al. (2006). In the NGC 2516 plot, the lines show $P = $ constant, $P \propto M^2$ and $P \propto M^3$, and the error bars show the median of the distribution binned in 0.1 dex bins of $\log M$.
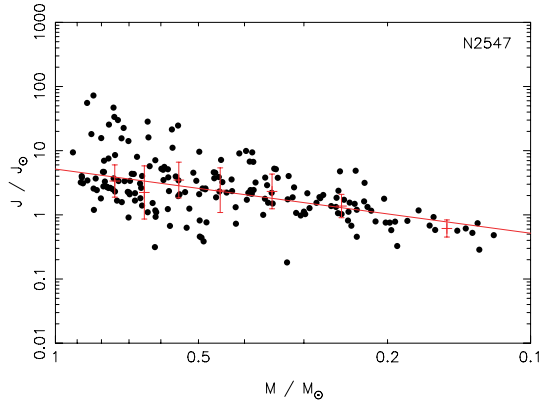
Figure 15. Stellar angular momentum *J* as a function of mass for the NGC 2547 rotation period sample. The error bars show the median of the distribution binned in 0.1 dex bins of $\log M$, and the solid line shows a fit of $J \propto M$ to the median.

envelope are treated as two separate entities joined at the convective/radiative boundary by angular momentum transfer according to the prescription of MacGregor (1991). The angular momentum loss rate was split into two components: losses due to stellar winds, assuming a loss law with saturation at a critical angular velocity ω_{sat} (allowed to vary as a function of mass), and losses due to disc locking, which to a good approximation maintains a constant angular velocity until the circumstellar disc dissipates at an age τ_{disc}. For the decoupled models there is one further parameter, τ_c, the time-scale for coupling of angular momentum between the core and envelope.

For NGC 2547, we have computed the object masses using two different values of the cluster parameters (particularly, the age), in order to examine the consistency of the rotation periods with the range of cluster ages found in the literature. The first set of parameters are those assumed earlier, corresponding to an age of 38.5 Myr, which is consistent with the lithium age for the cluster of ~35 Myr (Jeffries & Oliveira 2005). The second set of parameters corresponded to the 'conventional' isochrone-based estimates, from Naylor et al. (2002), with an age of 25 Myr, and corresponding distance modulus $(M - m)_0 = 8.05$.

6.2.2 Evolution from NGC 2362

We first attempt to evolve the observed rotation rates from our survey in NGC 2362 (Irwin et al. 2007c) forward in time to reproduce the available rotation period data. Following the method used in section 6.2.2 of Irwin et al. (2007b), we have characterized the slow rotator population by the 25th percentile (the lower quartile) of the distribution of observed angular velocities, ω, and the fastest rotators by the 90th percentile.

Fig. 16 shows a revised version of fig. 19 of Irwin et al. (2007b), adding in the NGC 2547 data. We have re-used the solid body and differentially rotating model fits to the NGC 2516 data: the models were *not* refit with the NGC 2547 observations. The mass bins used were as before: $0.9 < M/M_\odot \leqslant 1.1, 0.7 < M/M_\odot \leqslant 0.9, 0.5 < M/M_\odot \leqslant 0.7, 0.35 < M/M_\odot \leqslant 0.5$ and $0.2 < M/M_\odot \leqslant 0.35$ (chosen empirically to encompass the changes in behaviour seen in the models, while retaining reasonable statistics). The models were calculated for single masses roughly at the centre of these bins, of 1.0, 0.8, 0.6, 0.42 and 0.28 $M_\odot$. Since there are very few

observations (one) in the highest mass bin for NGC 2547, this will not be discussed further here.

Model parameters are summarized in each panel of Fig. 16. Briefly, we fit the models using NGC 2362 as an initial condition, to best reproduce the NGC 2516 rotation periods. The saturation angular velocity ω_{sat} and disc lifetime τ_{disc} were varied to obtain the best fit for the solid body models to the fast rotators, and for the decoupled models we varied τ_c, the core-envelope coupling time-scale, to fit the slow rotators. See Irwin et al. (2007b) for a more detailed discussion.

The models for the $0.7 < M/M_\odot \leqslant 0.9$ bin show overall good agreement with the NGC 2547 data. At this mass and age it is difficult to distinguish between the solid body and decoupled models, but at later ages, the solid body model appears to give a better fit to the rapid rotators, and a differentially rotating model to the slow rotators (Irwin et al. 2007b).

However, in the remaining three bins (and to some extent in the $0.7 < M/M_\odot \leqslant 0.9$ bin), a clear trend is visible for both the fast and slow rotator populations, where the observations show that the stars in NGC 2547 are rotating slower than expected.

Returning to Fig. 14, it is clear that the fastest rotators have spun up significantly from NGC 2362 to 2547, in accordance with the model prediction. Furthermore, there is some degree of scatter in the NGC 2362 data, especially at short periods, which may be due to contamination, e.g. from field binaries (Irwin et al. 2007c) in a similar fashion as we have hypothesized in M34 (Irwin et al. 2006) and NGC 2516 (Irwin et al. 2007b). If this is true, the presence of these objects has shifted the 90th percentile in NGC 2362 upward in ω, and may partly explain the discrepancy, especially due to the small number of objects in question. It is difficult to confirm this hypothesis before obtaining follow-up spectroscopy for the NGC 2362 sample to determine the nature of these objects.

For the slow rotators, examining Fig. 14 indicates that there are a number of 'outliers' at longer period than the general trend shown by the upper envelope of the rotators. It is possible that that if these objects were removed from the computation of the percentiles, the slow rotators would then fall into agreement with the models. The nature of these objects is not clear, and we defer discussion of them in detail until we can obtain spectroscopy to confirm their nature as slow rotators, and confirm the masses we have determined from the models of Baraffe et al. (1998).

Returning to the issue of the age of NGC 2547, the rotation periods seem to be slightly more consistent with the younger 25 Myr age, although the results are still clearly not reproduced by the models, especially in the intermediate-mass $0.5 < M/M_\odot \leqslant 0.7$ and $0.35 < M/M_\odot \leqslant 0.5$ bins, where the NGC 2547 objects appear to be rotating slower than the models predict. Moving the NGC 2547 points to the left-hand side in the diagram would improve agreement with the models, but this is difficult to justify since the youngest ages in the literature for this cluster are ~20–25 Myr. Given the uncertainties in the models, the rotation period measurements cannot therefore place useful constraints on the cluster age.

In light of the discussion above, the NGC 2547 data seem to be in reasonable agreement with the models, pending the results of spectroscopic follow-up, without need for significant modification from the earlier NGC 2516 study Irwin et al. (2007b). At this age it is difficult to observe the effects of core-envelope decoupling, so we are unable to refute our earlier statements that core-envelope decoupled models appear to be required to reproduce the evolution of the slowest rotators, and that the same models do not appear to give a good fit to the fast rotators, which are well fitted by solid body models.
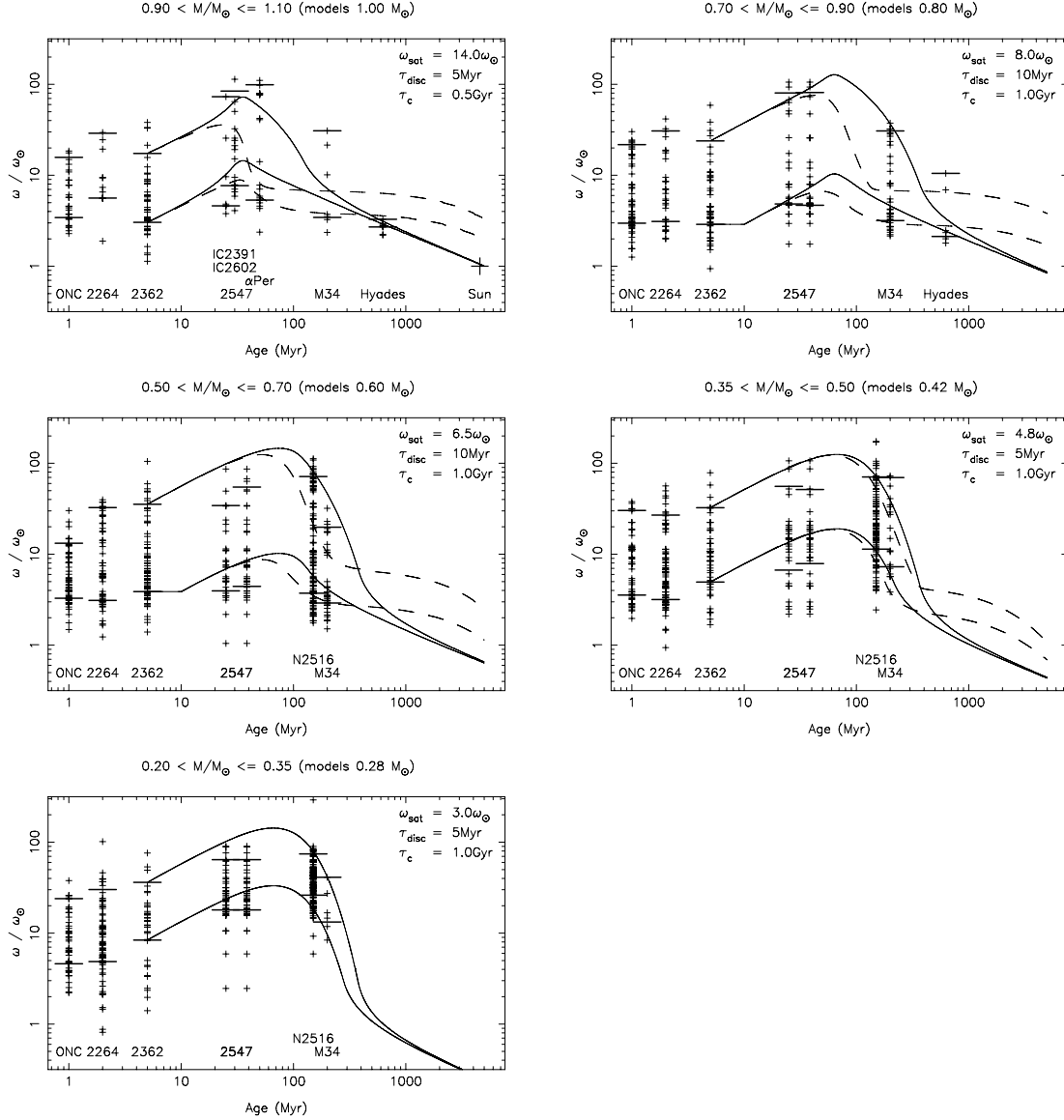
Figure 16. Rotational angular velocity ω plotted as a function of time in five mass bins: $0.9 < M/M_\odot \leqslant 1.1, 0.7 < M/M_\odot \leqslant 0.9, 0.5 < M/M_\odot \leqslant 0.7, 0.35 < M/M_\odot \leqslant 0.5$ and $0.2 < M/M_\odot \leqslant 0.35$. Crosses show the rotation period data, and short horizontal lines the 25th and 90th percentiles of ω, used to characterize the slow and fast rotators, respectively. The lines show our models for 1.0, 0.8, 0.6, 0.42 and $0.28\,M_\odot$ (respectively), where the solid lines are solid body models, and dashed lines are differentially rotating models, with the parameters shown. Plotted are the ONC (1 Myr), NGC 2264 (2 Myr), NGC 2362 (5 Myr), IC 2391, IC 2602 ($\sim$30 Myr), α Per ($\sim$50 Myr), NGC 2547 (plotted for ages of 25 and 38.5 Myr, as described in the text), M34, the Hyades (625 Myr) and the Sun ($\sim$4.57 Gyr). The IC 2391 data were taken from Patten & Simon (1996) and IC 2602 from Barnes et al. (1999). The α Per data are a compilation of the results from Stauffer et al. (1985), Stauffer, Hartmann & Jones (1989), Prosser et al. (1993a), Prosser (1991), Prosser et al. (1993b), O'Dell & Collier Cameron (1993), Prosser et al. (1995), O'Dell, Hendry & Collier Cameron (1994), O'Dell at al. (1996), Allain et al. (1996), Martín & Zapatero Osorio (1997), Prosser & Randich (1998), Prosser, Randich & Simon (1998), Barnes et al. (1998), and the Hyades data from Radick et al. (1987) and Prosser et al. (1995), taken from the open cluster data base.

6.2.3 Detailed evolution

Fig. 17 shows the results of attempting to evolve the measured rotation periods in NGC 2362 forward in time to the age of NGC 2547 using the models we have described, with the relations fit from the NGC 2516 data for ω_{sat} as a function of mass, on an object-by-object basis. By doing this, we can test if the model we have presented can reproduce the observations of NGC 2547, given the NGC 2362 rotators as an input.

Comparing the left- and right-hand panels in Fig. 17 indicates that the results are relatively independent of the assumed age for

NGC 2547. This is due to the relatively shallow slope of the time dependence in the rotation rates during this age range (see Fig. 16).

The shape of the mass-dependent morphology of the NGC 2547 distribution is reasonably well reproduced from the NGC 2362 distribution by the models, with the differentially rotating models providing a slightly better fit overall to the slow rotators, but at this age it is difficult to distinguish between the two classes of models since the effects of differential rotation become much more pronounced between $\sim$50–100 Myr.

Furthermore, the rotation rates are also well reproduced below $\sim$0.7 $M_\odot$, but not for higher masses, where the predicted rates are
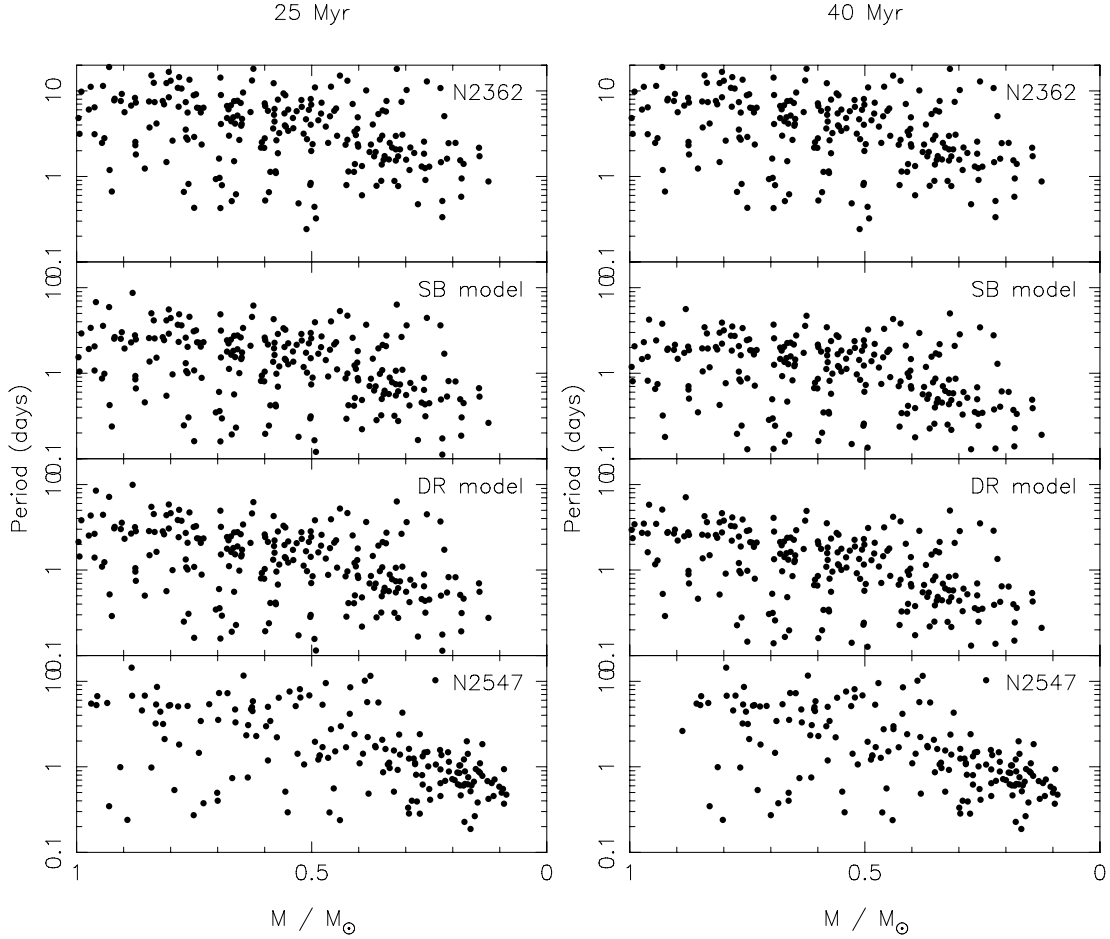
Figure 17. Rotation period as a function of mass, using the model presented in Section 6.2 to evolve the NGC 2362 distribution (top panel) forward in time from 5 Myr to 25 Myr (left-hand panels) and 40 Myr (right-hand panels) for the solid body (second panel) and differentially rotating (third panel) models, and the observed NGC 2547 distribution for comparison (bottom panel).

$\sim$ a factor of 2 faster than actually observed in NGC 2547. It should be noted that the adopted values of ω_{sat} in this mass range are not well constrained by the NGC 2516 data used to calibrate them, and have a strong effect on the morphology of this part of the diagram, so it is possible that any deviations here result from our assumption of a linear relation over the entire mass range.

The models predict that a number of objects should be rotating faster than $\sim$0.2 d, whereas none were observed in NGC 2547. However, re-examining Fig. 14 shows some scatter in the NGC 2362 distribution at short periods, which may be related to contamination of the sample, so it is difficult to conclude if this result is significant before obtaining follow-up of the NGC 2362 sample.

This work suggests overall that the mass dependence of the observed rotation period distribution is reasonably well reproduced by the combination of the initial conditions as seen in NGC 2362, the mass dependence of stellar contraction on the PMS, and the mass dependence of the saturation angular velocity ω_{sat}, in agreement with Irwin et al. (2007b).

7 CONCLUSIONS

We have reported on results of an *I*-band photometric survey of NGC 2547, covering $\sim$0.6 deg^2 of the cluster. Selection of candidate members in a *V* versus *V* − *I* CMD using an empirical fit to the

cluster sequence found 800 candidate members, over a *V* magnitude range of $12.5 < V < 24$ (covering masses from $0.9\,\text{M}_\odot$ down to below the brown dwarf limit). The likely field contamination level was estimated using a simulated catalogue of field objects from the Besançon Galactic models (Robin et al. 2003), finding that $\sim$470 objects were likely field contaminants, an overall contamination level of $\sim$59 per cent, implying that there are $\sim$330 real cluster members over this mass range in our FOV.

From $\sim$100 h of time-series photometry we derived light curves for $\sim$130 000 objects in the NGC 2547 field, achieving a precision of <1 per cent per data point over $14 \lesssim I \lesssim 18$. The light curves of our candidate cluster members were searched for periodic variability corresponding to stellar rotation, giving 176 detections over the mass range $0.1 < M/\text{M}_\odot < 0.9$.

The rotation period distribution as a function of mass was found to show a clear mass-dependent morphology, intermediate between those found in NGC 2362 (Irwin et al. 2007c) and NGC 2516 (Irwin et al. 2007b), with a median relation of $J \propto M$, or $j = $ constant, as seen in the other clusters we have surveyed.

In Section 6.2, simple models of the rotational evolution were considered, both for the solid body case, and including differential rotation between a decoupled radiative core and convective envelope, as in our earlier work on NGC 2516 (Irwin et al. 2007b). Allowing for the uncertainty in the age of NGC 2547, the results

indicate that it is possible to qualitatively reproduce the shape of the observed rotation rate distribution by evolving the NGC 2362 distribution forward in time, using the parameters fit to the NGC 2516 data of Irwin et al. (2007b). It is difficult to examine the effects of differential rotation at this age since they are still relatively small. Some small discrepancies were noted, caused by what appear to be 'outliers' in the distributions for NGC 2362 and 2547, but it is difficult to resolve these issues at the present time. Follow-up spectroscopy will be required to make further progress.

REFERENCES

Aigrain S., Hodgkin S., Irwin J., Hebb L., Irwin M., Favata F., Moraux E., Pont F., 2007, MNRAS, 375, 29
Allain S., Fernandez M., Martín E. L., Bouvier J., 1996, A&A, 314, 173
Baade D. et al., 1999, The Messenger, 95, 15
Balona L. A., Laney C. D., 1996, MNRAS, 281, 1341
Baraffe I., Chabrier G., Allard F., Hauschildt P. H., 1998, A&A, 337, 403
Barnes J. R., Collier Cameron A., Unruh Y. C., Donati J. F., Hussain G. A. J., 1998, MNRAS, 299, 904
Barnes S. A., Sofia S., Prosser C. F., Stauffer J. R., 1999, ApJ, 516, 263
Basri G., Martín E. L., 1999, ApJ, 510, 266
Chabrier G., Baraffe I., 1997, A&A, 327, 1039
Chabrier G., Baraffe I., Allard F., Hauschildt P. H., 2000, ApJ, 542, 464
Cieza L., Baliber N., 2006, ApJ, 649, 862
Getman K. et al., 2005, ApJS, 160, 319
Gorlova N., Balog Z., Rieke G. H., Muzerolle J., Su K. Y. L., Ivanov V. D., Young E. T., 2007, ApJ, 670, 516
Herbst W., Bailer-Jones C. A. L., Mundt R., 2001, ApJ, 554, 197
Herbst W., Bailer-Jones C. A. L., Mundt R., Meisenheimer K., Wackermann R., 2002, A&A, 396, 513
Hillenbrand L., 1997, AJ, 113, 1733
Hodgkin S. T., Irwin J. M., Aigrain S., Hebb L., Moraux E., Irwin M. J., 2006, Astron. Nachr., 327, 9
Irwin M. J., Lewis J. R., 2001, New Astron. Rev., 45, 105
Irwin J., Aigrain S., Hodgkin S., Irwin M., Bouvier J., Clarke C., Hebb L., Moraux E., 2006, MNRAS, 370, 954

Irwin J., Irwin M., Aigrain S., Hodgkin S., Hebb L., Moraux E., 2007a, MNRAS, 375, 1449
Irwin J. et al., 2007b, MNRAS, 377, 741
Irwin J., Hodgkin S., Aigrain S., Bouvier J., Hebb L., Irwin M., Moraux E., 2007c, MNRAS, preprint (arXiv:0711.2398)
Jeffries R. D., 1999, in Butler C. J., Doyle J. G., eds, ASP Conf. Ser. Vol. 158, Solar and Stellar Activity: Similarities and Differences. Astron. Soc. Pac., San Francisco, p. 75
Jeffries R. D., Oliveira J. M., 2005, MNRAS, 358, 13
Jeffries R. D., Tolley A. J., 1998, MNRAS, 300, 331
Jeffries R. D., Totten E. J., James D. J., 2000, MNRAS, 316, 950
Jeffries R. D., Thurston M. R., Hambly N. C., 2001, A&A, 375, 863
Jeffries R. D., Oliveira J. M., Barrado y Navascués D., Stauffer J. R., 2003, MNRAS, 343, 1271
Jeffries R. D., Naylor T., Devey C. R., Totten E. J., 2004, MNRAS, 351, 1401
Jeffries R. D., Evans P. A., Pye J. P., Briggs K. R., 2006, MNRAS, 367, 781
Jones B. F., Prosser C. F., 1996, AJ, 111, 1193
Jones B. F., Fischer D. A., Stauffer J. R., 1996, AJ, 112, 1562
Krishnamurthi et al., 1998, ApJ, 493, 914
Lamm M. H., Mundt R., Bailer-Jones C. A. L., Herbst W., 2005, A&A, 430, 1005
Landolt A. J., 1992, AJ, 104, L340
Leggett S. K., 1992, ApJS, 82, 351
Leggett S. K., Allard F., Berriman G., Dahn C. C., Hauschildt P. H., 1996, ApJS, 104, 117
Littlefair S. P., Naylor T., Jeffries R. D., Devey C. R., Vine S., 2003, MNRAS, 345, 1205
MacGregor K. B., 1991, in Catalano S., Stauffer J. R., eds, Angular Momentum Evolution of Young Stars. Kluwer Academic Publishers, Dordrecht
Magnitskii A. K., 1987, Sov. Astron. Lett., 13, 451
Makidon R. B., Rebull L. M., Strom S. E., Adams M. T., Patten B. M., 2004, AJ, 127, 2228
Martín E. L., Zapatero Osorio M. R., 1997, MNRAS, 286, L17
Mayor M., 1974, A&A, 32, 321
Meusinger H., Stecklum G., Reimann H. G., 1991, A&A, 245, 57
Meynet G., Mermilliod J.-C., Maeder A., 1993, A&AS, 98, 477
Moitinho A., Alves J., Huélamo N., Lada C. J., 2001, ApJ, 563, 73
Naylor T., Jeffries R., 2006, MNRAS, 373, 1251
Naylor T., Totten E. J., Jeffries R. D., Pozzo M., Devey C. R., Thompson S. A., 2002, MNRAS, 335, 291
Noyes R. W., Hartmann L. W., Baliunas S. L., Duncan D. K., Vaughan A. H., 1984, ApJ, 279, 763
O'Dell M. A., Collier Cameron A., 1993, MNRAS, 262, 521
O'Dell M. A., Hendry M. A., Collier Cameron A., 1994, MNRAS, 268, 181
O'Dell M. A., Hilditch R. W., Collier Cameron A., Bell S. A., 1996, MNRAS, 284, 874
Oliveira J. M., Jeffries R. D., Devey C. R., Barrado y Navascués D., Naylor T., Stauffer J. R., Totten E. J., 2003, MNRAS, 342, 651
Park B., Sung H., Bessell M., Kang Y., 2000, AJ, 120, 894
Patten B., Simon T., 1996, ApJS, 106, 489
Pizzolato N., Maggio A., Micela G., Sciortino S., Ventura P., 2003, A&A, 397, 147
Preibisch T. et al., 2005, ApJS, 160, 401
Prosser C. F., 1991, PhD thesis, Univ. California, Santa Cruz
Prosser C. F., Randich S., 1998, Astron. Nachr., 319, 210
Prosser C. F., Schild R. E., Stauffer J. R., Jones B. F., 1993a, PASP, 105, 269
Prosser C. F. et al., 1993b, PASP, 105, 1407
Prosser C. F. et al., 1995, PASP, 107, 211
Prosser C. F., Randich S., Simon T., 1998, Astron. Nachr., 319, 215
Queloz D., Allain S., Mermilliod J.-C., Bouvier J., Mayor M., 1998, A&A, 335, 183
Radick R. R., Thompson D. T., Lockwood G. W., Duncan D. K., Baggett W. E., 1987, ApJ, 321, 459
Randich S., 2000, in Pallavicini R., Micela G., Sciortino S., eds, ASP Conf. Ser. Vol. 198, Stellar Clusters and Associations: Convection, Rotation and Dynamos. Astron. Soc. Pac., San Francisco, p. 401

Robin A. C., Reylé C., Derrière S., Picaud S., 2003, A&A, 409, 523

Scholz A., Eislöffel J., 2004, A&A, 421, 259

Soderblom D. R., Stauffer J. R., Hudon J. D., Jones B. F., 1993, ApJS, 85, 315

Stauffer J. R., Hartmann L. W., 1987, ApJ, 318, 337

Stauffer J. R., Hartmann L., Soderblom D. R., Burnham N., 1984, ApJ, 280, 202

Stauffer J. R., Hartmann L. W., Burnham J. N., Jones B. F., 1985, ApJ, 289, 247

Stauffer J. R., Schild R. A., Baliunas S. L., Africano J. L., 1987, PASP, 99, 471

Stauffer J. R., Hartmann L. W., Jones B. F., 1989, ApJ, 346, 160

Terndrup D. M., Krishnamurthi A., Pinsonneault M. H., Stauffer J. R., 1999, AJ, 118, 1814

Terndrup D. M., Stauffer J. R., Pinsonneault M. H., Sills A., Yuan Y., Jones B. F., Fischer D., Krishamurthi A., 2000, AJ, 119, 1303

Terndrup D. M., Pinsonneault M., Jeffries R. D., Ford A., Sills A., 2002, ApJ, 576, 950

Van Leeuwen F., Alphenaar P., Meys J. J. M., 1987, A&AS, 67, 483

Young E. T. et al., 2004, ApJS, 154, 428

SUPPLEMENTARY MATERIAL

The following supplementary material is available for this article:

Table 1. Properties of our 176 rotation candidates. The period P in days, i-band amplitude α_i (units of magnitudes, in the instrumental bandpass), interpolated mass and radius (from the models of Baraffe et al. 1998, derived using the I magnitudes) are given (where available). Our identifiers are formed using a simple scheme of the cluster name, field number, CCD number and a running count of stars in each CCD, concatenated with dashes. Machine-readable copies of the data tables from all the Monitor rotation period publications are also available at http://www.ast.cam.ac.uk/research/monitor/rotation/.

This material is available as part of the online article from: http://www.blackwell-synergy.com/doi/abs/10.1111/j.1365-2966.2007.12669.x (this link will take you to the article abstract).

Please note: Blackwell Publishing are not responsible for the content or functionality of any supplementary materials supplied by the authors. Any queries (other than missing material) should be directed to the corresponding author for the article.

This paper has been typeset from a TEX/LATEX file prepared by the author.